Numerical Modeling of a Coastal Trapped Disturbance. Part I: Comparison with Observations

SHUCAI GUAN AND PETER L. JACKSON

Environmental Studies Program, University of Northern British Columbia, Prince George, British Columbia, Canada

CHRIS J. C. REASON

School of Earth Sciences, University of Melbourne, Melbourne, Australia

(Manuscript received 29 October 1996, in final form 11 July 1997)

ABSTRACT

The coastal trapped disturbance (CTD) of 15–17 May 1985 represents an example of a strong mesoscale trapped event along the west coast of North America with abrupt transitions in many basic meteorological parameters. In this study, a comparison between observations and a numerical simulation of this event using the Regional Atmospheric Modeling System (RAMS) is presented. The model is shown to realistically reproduce CTD characteristics such as the coastal transition from northerly to southerly flow, as a mesoscale coastal ridge of higher pressure with associated drops in marine-layer temperature propagates northward along the west coast of North America. Simulated sea level pressure and temperature fields near the surface match well with observations, especially at the synoptic scale. The model realistically simulates mesoscale sea level pressure and 6-h pressure changes during the event. The modeled hourly time evolution of sea level pressure and the southerly transitions at a series of coastal stations and buoys also agree reasonably well with observations. The marine boundary layer is not well initialized or very well represented in the model, suggesting that, for this particular case, the details of the boundary layer are not crucial in the evolution of the CTD. It is suggested that the RAMS model can be usefully applied to investigate CTD evolution.

1. Introduction

Coastal trapped disturbances (CTDs) are mesoscale systems that are laterally confined against a coastal mountain barrier by Coriolis effects and vertically confined by stable stratification. CTDs propagate along the coastal mountain barrier such that the barrier is on the right (left) in the Northern (Southern) Hemisphere. Propagation is generally energetic but relatively short lived (typically 2–3 days on the North American west coast). Typical length scales are 1000 km alongshore, 100 km across-shore, and 0.1 km in the vertical (Reason 1994).

CTDs along the west coast of North America are generally coastal ridges of higher pressure in the marine layer (Dorman 1985, 1987; Mass and Albright 1987; Reason and Dunkley 1993). Similar coastal ridges have been observed in southeastern Australia (Holland and Leslie 1986), whereas CTD events in southern Africa are typically mesoscale coastal lows (Gill 1977; Reason and Jury 1990). In all areas, CTDs may occur several times per month during the summer and less frequently during the winter. CTDs usually cause significant changes to coastal weather. Clear skies are replaced by stratus, and sometimes fog and drizzle; marine-layer air cools by as much as 20°C; and sudden wind shifts (along the North American west coast from northerly to southerly) with gusts up to 20 m s^{-1} or more often occur (e.g., Dorman 1985; Mass and Albright 1987; Reason and Dunkley 1993). These changes typically happen over periods of minutes to hours with varying strength and are often intensified in the vicinity of prominent capes, such as Point Conception or Cape Mendocino.

Because of the frequency of CTD events, and the rapidity and intensity of their associated weather changes, it is clear that CTDs represent a formidable forecast problem (Reason and Steyn 1990). Forecasting the evolution of CTD events is often made more difficult by the poorly understood unsteady propagation of CTDs in the vicinity of coastlines with complex topography (Reason and Dunkley 1993).

CTDs have been variously interpreted as 1) the mesoscale response to alongshore pressure gradients created by the interaction between synoptic-scale flow and coastal topography (Mass et al. 1986; Mass and Albright 1987), 2) coastally trapped gravity currents (Dorman

Corresponding author address: Dr. Peter L. Jackson, Environmental Studies Program, Faculty of Natural Resources and Environmental Studies, University of Northern British Columbia, 3333 University Way, Prince George, BC V2N 4Z9, Canada.
E-mail: peterj@unbc.edu

TABLE 1. Grid sizes and dimensions. Note that the ΔZ specified is the value at the surface. The vertical resolution gradually stretches by a ratio of 1.2 at each successive level until a maximum value of 1000 m is reached. The vertical domain stretches from the surface to 16.5 km ASL.

	Nx	Ny	Nz	$\Delta X = \Delta Y$ (km)	ΔZ (m)	Δt (s)
Grid 1	35	35	32	100	75	90
Grid 2	58	78	32	25	75	30
Grid 3	34	158	47	6.25	18.75	10

1987; Mass and Albright 1987), and 3) freely propagating Kelvin waves (Dorman 1985, 1988). Reason and Steyn (1992) presented a theoretical framework for interpreting these events and suggested that both synoptic-scale effects and marine- boundary-layer responses are important in the initiation and propagation of these disturbances. This framework included both a nonlinear Kelvin wave component and a trapped gravity current, both of which evolve in response to the alongshore pressure gradient. Rogerson and Samelson (1995) presented a reduced-gravity model of a CTD that suggested that unsteady propagation of these events can also occur as the linear response to upper-level synoptic forcing. Shallow-water numerical modeling studies (Klemp et al. 1995) have suggested that Kelvin waves can evolve to acquire gravity current characteristics. The variations in interpretation of these events are further reflected in the climatological study of Bond et al. (1996), which found that CTDs in Oregon and Washington tended to be characterized by more abrupt changes (consistent with a gravity current interpretation) than those farther south (consistent with a Kelvin wave interpretation).

While the theoretical studies (Klemp et al. 1995; Reason and Steyn 1992; Rogerson and Samelson 1995) can capture the basic features of CTD events and are useful for investigating particular processes, it is necessary to use a high-resolution numerical model to investigate the mesoscale details of these events. Such mesoscale numerical simulations are also needed to investigate the sensitivity of CTD events to factors such as variability in the topography, surface fluxes, and in the background synoptic conditions that various observational studies have suggested are important for CTD evolution and decay.

As a necessary first step, the purpose of this study is to analyze a numerical simulation of a particular CTD event along the west coast of North America, namely, that of 15–17 May 1985, in conjunction with the observations of this event reported in Mass and Albright (1987, hereafter MA87). The numerical model used in this study was the Colorado State University Regional Atmospheric Modeling System (RAMS). As far as we are aware, this effort represents one of very few attempts to simulate an actual observed CTD event with a 3D mesoscale model. We have chosen to simulate the May 1985 event because it represents an example of a strong

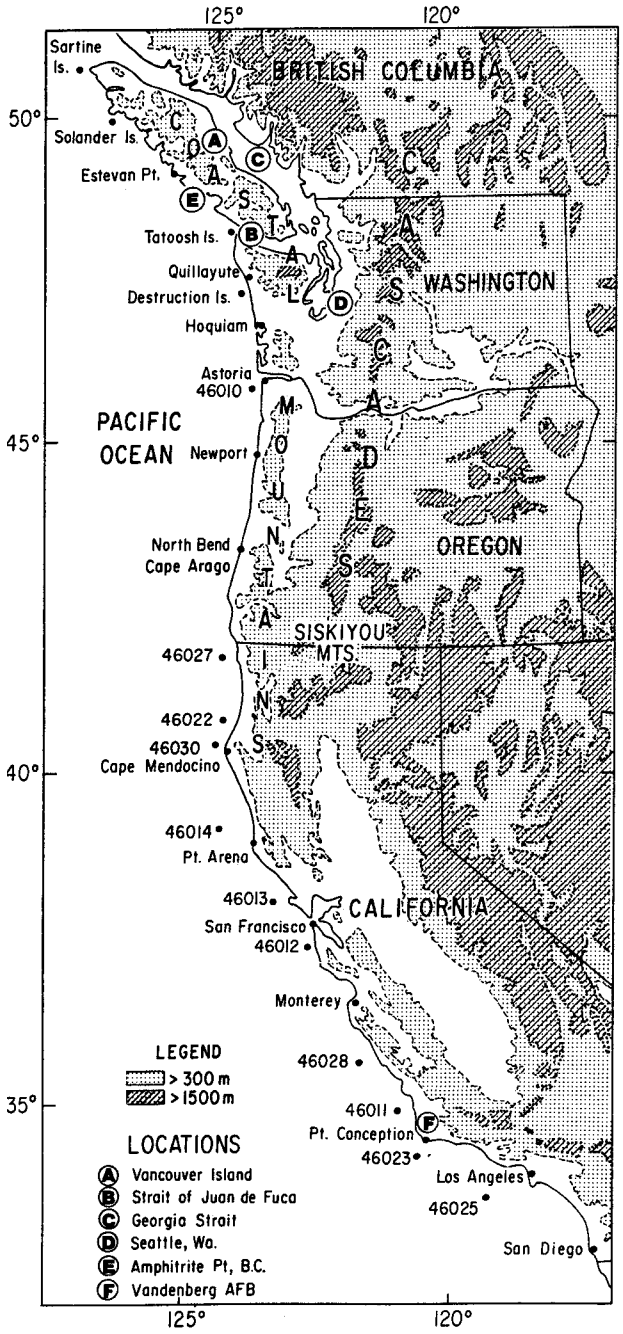

FIG. 1. Location and topographic configuration. (Reproduced from MA87's Fig. 1.)

CTD (e.g., Bond et al. 1996) for which a reasonable amount of mesoscale observational data exists (MA87). Unlike some other CTD events on the U.S. west coast [e.g., the May 1982 case in California—Dorman (1985, 1988); MA87, Mass and Albright (1988)], the dynamical interpretation of the May 1985 case has been reasonably straightforward and not subject to ambiguity and controversy. The focus herein is on a comparison between the observed and model fields with detailed

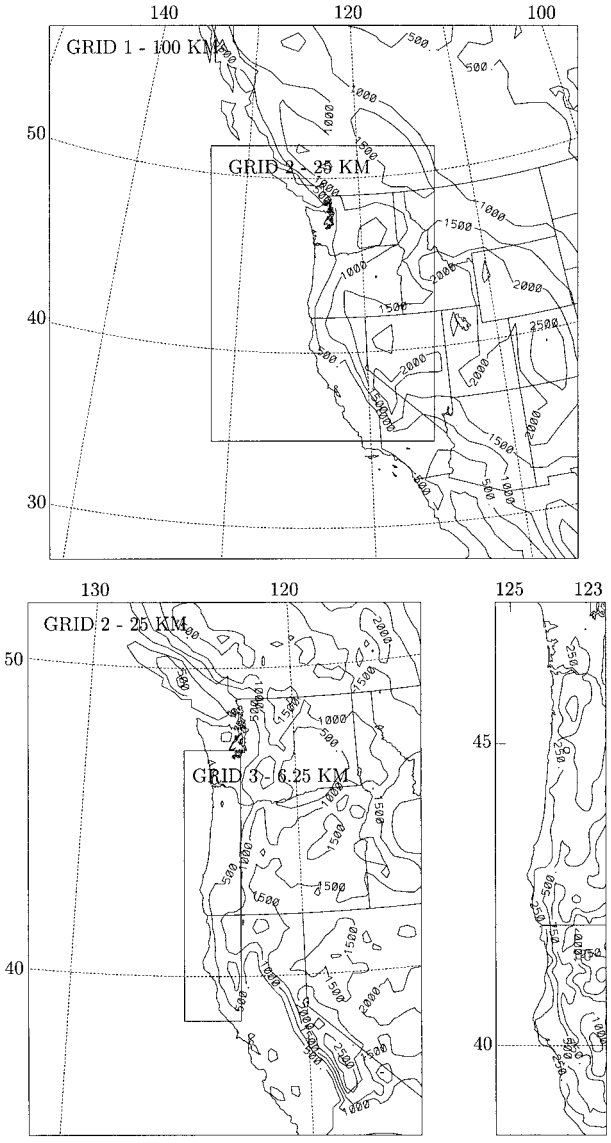

FIG. 2. Location and extent of nested grids used in RAMS simulation.

analysis of the dynamical balances in effect during the initiation and propagation of the event forming the subject of a companion study.

2. Model description

Details of RAMS, used to simulate the CTD event, are described in Pielke et al. (1992). RAMS is a versatile mesoscale model allowing tailored applications to a wide range of atmospheric phenomena. Pielke et al. (1992) review applications of RAMS ranging from large eddy simulations, simulations of thunderstorms, mesoscale convective systems, midlatitude cirrus clouds, and winter storms through to thermally and mechanically forced mesoscale flows and mesoscale atmospheric dispersion.

Some examples of RAMS applications to modeling mesoscale flows are sea breezes (e.g., Xian and Pielke 1991), cold surges along the Front Range of the Rocky Mountains (e.g., Abbs and Pielke 1987), gap winds in British Columbian fjords (e.g., Jackson and Steyn 1994), and the interaction between standing mountain waves and cold pools (Lee et al. 1989).

The particular RAMS configuration used for this CTD simulation includes the following options: nonhydrostatic; horizontally variable initial conditions and time-dependent lateral boundary conditions on grid 1; moisture can condense as cloud, but no ice or precipitation mechanisms are present (precipitation was not observed during the event); rigid-lid upper-boundary condition; solar and terrestrial radiation permitted on all grids (computed every 1200 s); semi-implicit acoustic model; Arakawa type-C grid stagger; second-order leapfrog differencing for velocity and pressure and second-order forward differencing for all other prognostic variables; 11 grid levels in the soil ranging down to 0.5 m below the surface; and surface roughness length of 0.05 m over land, and roughness length computed from wind speed over water.

Three grids were nested to allow the horizontal grid spacing to vary from 100 km (required to efficiently resolve the synoptic-scale) to 6.25 km (required to resolve the mesoscale). The grid dimensions and time steps are shown in Table 1. Vertically, grids 1 and 2 have the same 32 levels with vertical grid spacing starting at 75 m at the surface and stretching by a factor of 1.2 for each successive level above the surface to a maximum separation of 1000 m, which resulted in a vertical domain of 16.5 km. Grid 3 has 47 vertical levels and has spacing four times finer than the other grids (18.75 m at the surface) near the surface. Realistic synoptic initial conditions are imposed by choosing the RAMS initialization option to be horizontally variable (as opposed to horizontally homogeneous) so that initial gradients can vary horizontally across the domain. The data used to initialize (and provide lateral boundary conditions for) RAMS grid 1 were interpolated from the 0-h prognosis at 2.5° horizontal spacing of the National Centers for Environmental Prediction (NCEP) model. The lateral and top boundaries of grid 1 were time variable and were nudged toward the NCEP fields using a Newtonian relaxation scheme with an *e*-folding timescale of 1000 s. The interior of grid 1 was nudged with an *e*-folding timescale of 5000 s.

The RAMS nesting scheme implements two-way interaction, as described by Clark and Farley (1984). Thus grid 2 obtains only its lateral boundary conditions from grid 1, and the average of its interior values overwrite those of grid 1. In the same way grid 3 obtains only its lateral boundary conditions from grid 2, and the average of its interior values overwrite those of

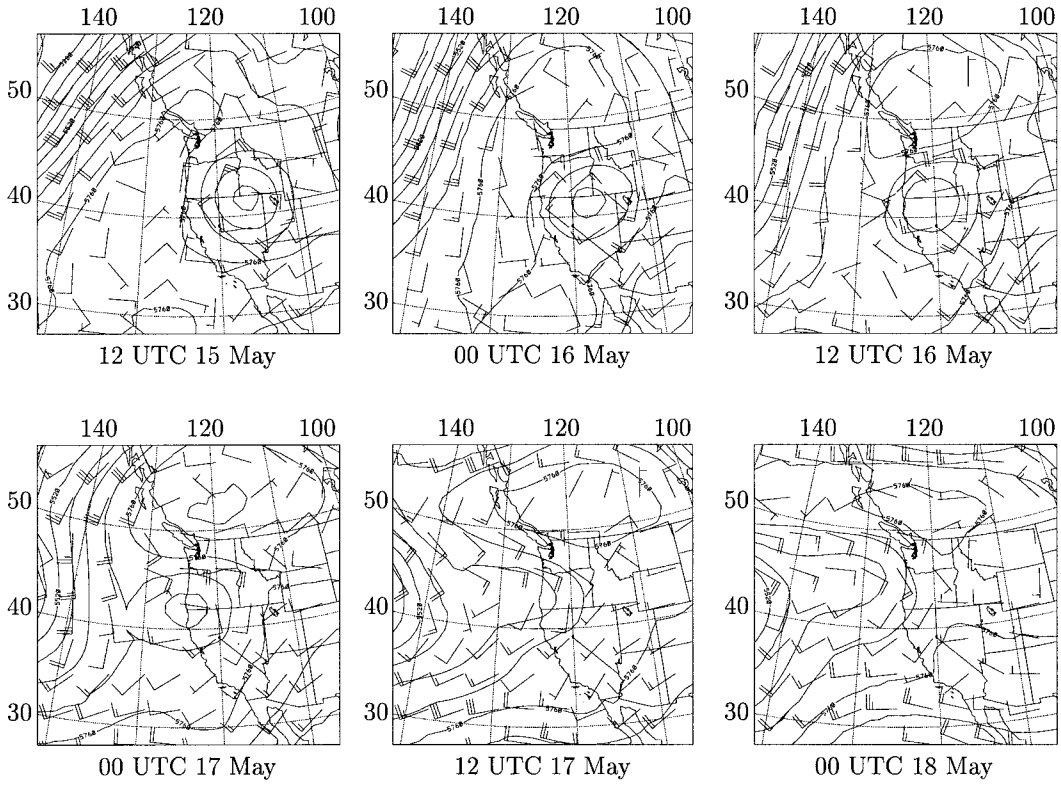

FIG. 3. Geopotential heights and winds at 500 hPa from NCEP data for the event of 15–17 May 1985. Contour interval is 60 m.

grid 2. The finer-resolution grids are initialized by interpolation from grid 1.

3. Comparison of observations with model simulation

a. Introduction

The CTD of 15–17 May 1985 that occurred along the California and Pacific Northwest coasts is an example of a strong event with an abrupt coastal transition in wind direction, wind speed, temperature, and sea level pressure. This event brought a wind shift from moderate northerlies (0–10 m s^{-1}) to southerlies of 15 m s^{-1} or more, temperature falls exceeding 10°C, and abrupt pressure rises in a period of less than 1 h (MA87). The wind reversal and coastal ridge of higher pressure during the CTD propagated from California to northern Vancouver Island, British Columbia; Fig. 1 details locations and topographic configuration of the region.

Previous modeling studies of CTD events have tended to use idealized shallow-water formulations [e.g., Reason and Steyn (1992); Klemp et al. (1995); Rogerson and Samelson (1995)]. A significant difficulty in attempting a simulation of an actual event with a sophisticated mesoscale numerical model such as RAMS is that the mesoscale nature of the ridges presents problems in obtaining observed data of sufficiently high spatial and temporal resolution 1) to properly initialize the numerical model and 2) to compare with the simulated results. A further difficulty is that a CTD usually brings abrupt transitions in many basic meteorological parameters over periods of minutes to hours. The details of these abrupt transitions can be quite difficult to simulate in a mesoscale numerical model and necessitate the use of nested high-resolution grids. Since such fine-grid simulations are computationally very expensive, there is a trade-off between simulation accuracy and resources required to produce the simulation. The simulation here uses three nested grids with the finest grid having a resolution of 6.25 km (Table 1) in a narrow coastal strip extending from central California to southern Washington (see Fig. 2). Bearing in mind these difficulties, we will compare the simulated CTD of 15–17 May 1985 with MA87 analyses of this event in synoptic, mesoscale, and time series variations.

b. Synoptic evolution and comparison

Figures 3 and 4 display geopotential heights and winds at 500 hPa from the NCEP data and our numerical simulations for the event of 15–17 May 1985, respectively. At 1200 UTC 15 May, both sets of geopotential height fields indicated that a high-amplitude ridge was present over the eastern North Pacific ex-

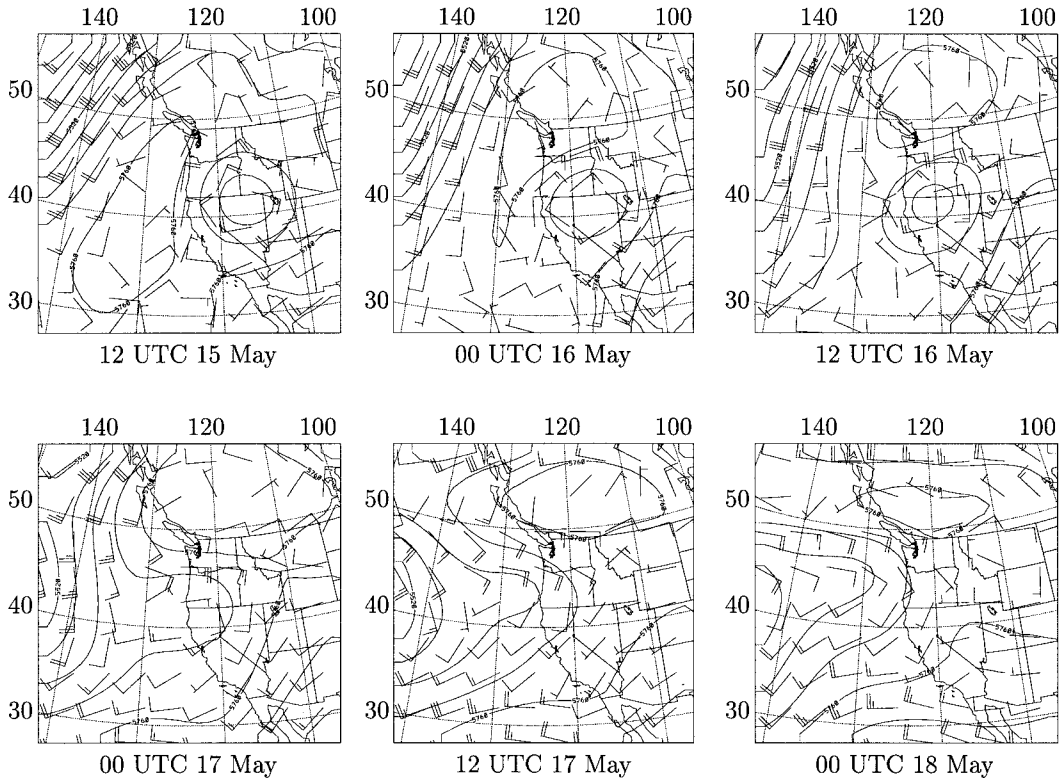

FIG. 4. Simulated geopotential heights and winds at 500 hPa for the event of 15–17 May 1985 from grid 1 with horizontal grid spacing of 100 km. For clarity, every fourth wind vector in both dimensions is plotted. Contour interval is 60 m.

tending into British Columbia and that a closed low was centered over northern Nevada. After 12 h (0000 UTC 16 May) the high drifted northeast and the closed low moved slightly westward. During the next 36 h (through 0000 UTC 18 May) the closed low slowly drifted westward, eventually becoming an open trough that split the ridge. Comparison of Figs. 3 and 4 suggests that the simulated geopotential heights and winds at 500 hPa for the event of 15–17 May 1985 matched the corresponding NCEP 500-hPa charts well. This result is not too surprising since the lateral boundaries and, to a lesser extent, the interior of RAMS grid 1 were relaxed toward the NCEP conditions. All other fields on grid 1 at other levels show the same degree of similarity with the NCEP data; thus, only the model fields are shown when discussing the synoptic evolution in this section.

The evolution of simulated geopotential heights and winds at 850 hPa are shown in Fig. 5. The 850-hPa chart for 1200 UTC 15 May indicates a closed high centered over British Columbia with a low centered over Nevada. During the event the high slid to the east-southeast, while the low moved to the west-northwest.

Figure 6 displays the simulated sea level pressure for 1200 UTC 15 May through 0000 UTC 18 May 1985. At 1200 UTC 15 May, high sea level pressure was centered over British Columbia and a trough extended northwestward from southeastern California to the coast. Over the next 2 days the high drifted southeastward, while a low moved westward from California into the Pacific and a high developed west of the Southern California Bight. Resulting from these synoptic changes, a narrow coastal pressure ridge (the CTD) evolved and traveled northward along the coast.

Figure 7 gives the modeled temperature field at 109.7 m above sea level (ASL). At 1200 UTC 15 May there was a weak cool centered 400 km west of San Diego with a warm area centered along the coast of southern California. Linked with the movement westward of the surface low, the warm area spread northward reaching coastal British Columbia by 1200 UTC 17 May. At the same time the cool area associated with the surface ridge moved north up the California coast.

In this section we have described the evolution of simulated geopotential heights, winds, and temperatures at 500 and 850 hPa, as well as sea level pressure for the CTD of 15–17 May 1985. Comparison of simulated fields with NCEP data indicates that the model, as expected given the time-dependent forcing on grid 1, does an excellent job in simulating the synoptic variations of geopotential heights, winds, and temperatures for the May 1985 CTD.

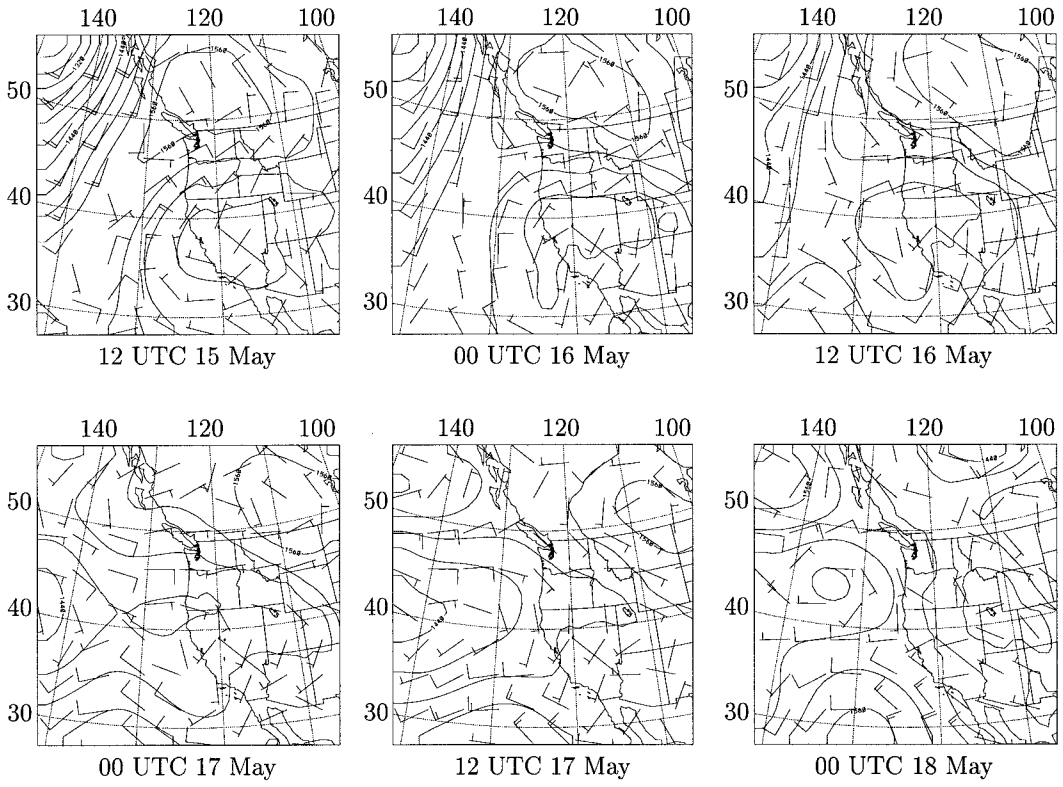

FIG. 5. Simulated geopotential heights and winds at 850 hPa for the event of 15–17 May 1985 from grid 1. For clarity, every fourth wind vector in both dimensions is plotted. Contour interval is 30 m.

c. Mesoscale evolution and comparison

Figure 8 shows the simulated sea level pressure and wind fields at the 109.7-m elevation for grid 2 (25-km horizontal resolution). At 1200 UTC 15 May, high pressure dominated the northwest corner of the domain, and a trough was positioned over central and coastal California. Northerly flow occurred offshore of the coastal mountains south of the Washington–British Columbia border. During the next 12 h (through 0000 UTC 16 May), a coastal pressure ridge (the CTD) began to form in southern California and the coastal winds shifted to southerly there. A coastal minimum in sea level pressure was located just north of the pressure ridge. In the following 30 h (through 0600 UTC May 17), the coastal trapped ridge strengthened and extended northward. As this ridge tracked north along the coast, the zone of southerly winds extended to reach southern Vancouver Island by 1800 UTC 17 May.

MA87 used the data of all available ship, buoy, and land stations and analyzed the mesoscale sea level pressure for the same event (their Fig. 9 reproduced here as Fig. 9). A comparison of their analyses with our simulations (Fig. 8) indicates that the model can realistically simulate the observed coastal ridge and wind reversal, as well as their propagation northward along the coast. Note that the simulated processes slightly lag the observations and that the simulated coastal pressure ridge is smoother than the ridge analyzed by MA87.

Figure 10 presents 6-h pressure changes of the simulated sea level pressures during the May 1985 CTD. This figure should be compared with Fig. 11, which is reproduced from MA87's Fig. 11. At 1800 UTC 15 May and 0000 UTC 16 May, there were pressure rises in southern California and pressure falls elsewhere. Over the next 18 h to 1200 UTC 16 May, pressure rose over the land and fell over the ocean as the thermal trough over interior California and the synoptic low moved out over the North Pacific (Fig. 6). By 1800 UTC 16 May, there were weak pressure rises along the California coast and large pressure falls over the continent extending north from northern California. The panel for 0000 UTC 17 May shows that the pressure tendencies at this stage were weakly positive south of the California–Oregon border region and weakly negative north of this region. However, over the next 6 h, the area of weak positive tendencies extended to cover all the domain (and similarly for 1200 UTC 17 May), as the CTD reached central Vancouver Island. The last panel (1800 UTC 17 May) shows a very weak positive tendency everywhere along the coast, and significant negative tendency inland, as the synoptic situation changed and the event came to an end. Examination of the isallobaric analyses

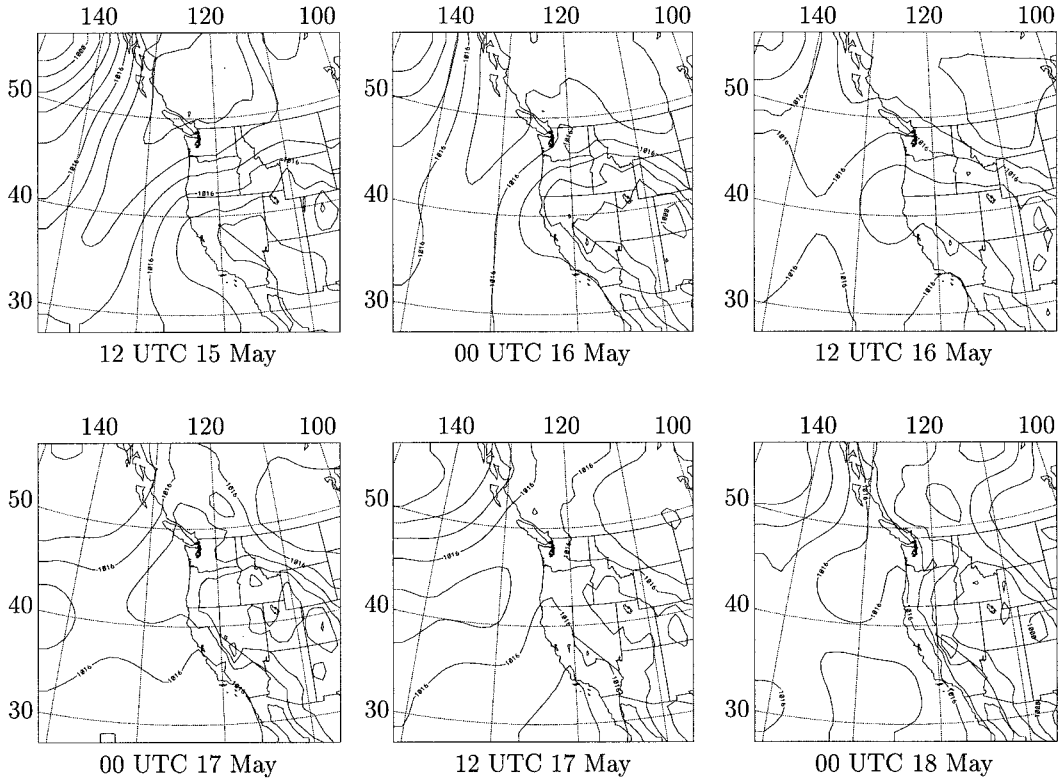

FIG. 6. Simulated sea level pressure for the event of 15–17 May 1985 from grid 1. Contour interval is 4 hPa.

of 6-h pressure changes in MA87 (Fig. 11) indicates that the model does a reasonable job in reproducing the pressure tendencies observed during the event.

Figure 12 shows the simulated sea level pressure with winds at the 108.4-m elevation for the domain of grid 3 (6.25-km horizontal resolution), which should also be compared with Fig. 9. (Note that the domain of our grid 3 is smaller than the domain in Fig. 9.) Prior to CTD onset (at 1200 UTC 15 May), both simulation and observation indicate that maximum surface coastal pressure was in the north of the domain with a strong alongshore gradient. As a result, northerly flow prevailed along the California and Pacific Northwest coasts. The simulated coastal pressure in the domain varied from 1010 to 1025 hPa, which matched very well with the corresponding observed values. By 0000 UTC 16 May both observed and simulated sea level pressures decreased and the pressure gradient along the northern California coast became small with a coastal pressure minimum located near the California–Oregon border. Ridging and the associated transition to southerly flow to the south of the coastal pressure minima continued during the next 12 h. By 0600 UTC 17 May, the coastal pressure decreased in the northern part of the model domain (southern Washington) and increased in the southern part. The coastal ridge of higher pressure and associated southerly flow moved northward along the coast so that by 1200 UTC 17 May the entire grid 3 domain was in southerly flow. Grid 3 simulated coastal pressure gradients, values, and trends matched well with observations.

The temperature evolution at the 108.4-m elevation in grid 3 of the model is shown in Fig. 13. At 1200 UTC 15 May cool air lay over southern Washington, while higher temperatures occurred over central California. During the next 12-h (through 0000 UTC 16 May) the temperature in the whole domain increased and temperature contours rotated counterclockwise to parallel the coastline. By 0600 UTC 16 May the rotation of the contours continued with cooler temperatures now appearing in the south, reversing the orientation of the initial temperature perature gradient. During the next 12 h (through 1800 UTC 16 May), the isotherms oriented across-shore with cool temperature to the south moved slowly northward. At 0000 UTC 17 May, the temperature field along the coast was the reverse of that found at 1200 UTC 15 May with warm conditions along southern Washington and cold along central California forming a large alongshore temperature gradient. The significant warming that occurred along the Oregon and southern Washington coasts between 1200 UTC 15 May and this time appears to be associated with offshore flow and its evolution ahead of the CTD during this period (Fig. 12). Both adiabatic warming of the flow originating from the interior mountains and warm advection may contribute to the temperature increase along the

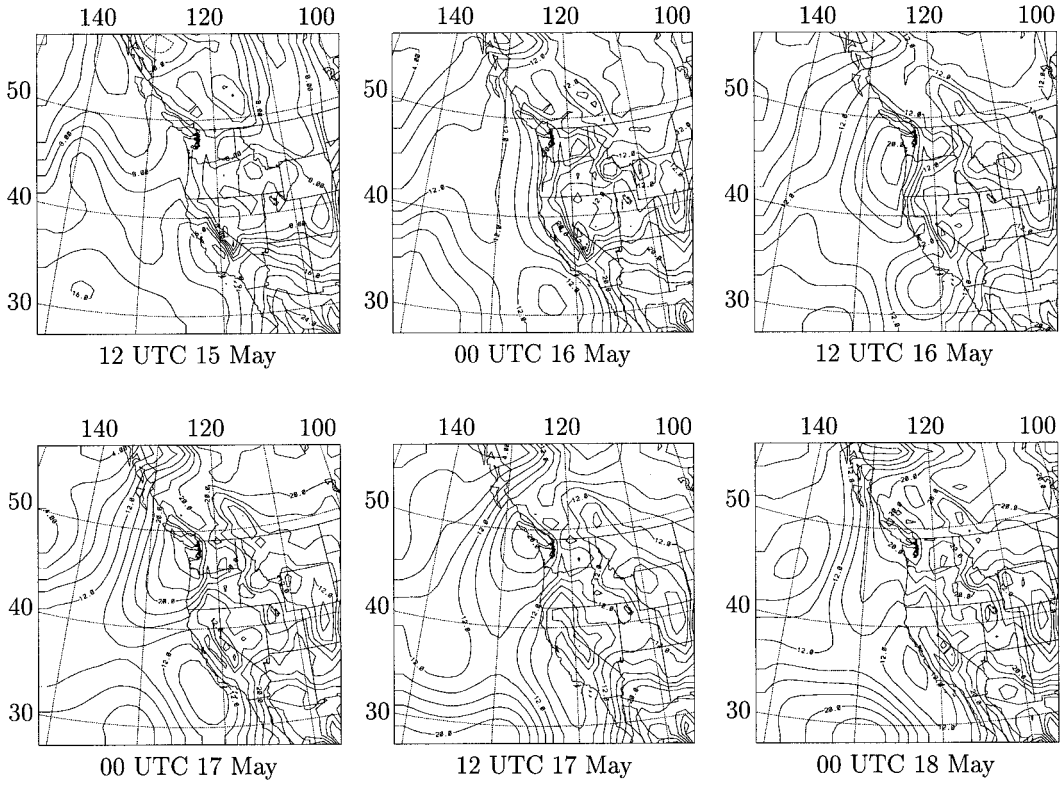

FIG. 7. Simulated temperature fields at 109.7 m above the surface for the event of 15–17 May 1985 from grid 1. Contour interval is 2°C.

coast. During the next 24-h (through 0000 UTC 18 May), the north of the model domain remained warm and the south cold, but the temperature gradient gradually decreased. The formation of cold air in the south and its propagation northward along the coast is related to the coastal ridging and southerly flow of the evolving CTD (Fig. 12).

d. Time series

The simulated time evolution of sea level pressure at a series of coastal stations and buoys from central California to the northern tip of Vancouver Island is shown in Fig. 14. The observed hourly time evolution of measured sea level pressure at those stations and buoys for the same event is shown in Fig. 15 (reproduced from MA87, Fig. 12). Both the simulation and observations show that sea level pressure for the central California locations (buoys 46012 and 46013, Point Arena) fell to about 1009 hPa and then slowly rose to about 1020 hPa during the event. Despite the fact that the simulated pressures arrived at their minima a couple of hours later and reached their maxima a few hours earlier than those observed, the simulated time evolution of sea level pressure for the central California locations matched reasonably well with the observations. The simulated time evolution of sea level pressure at buoy 46022 was also very similar to the observations with a maximum pressure of approximately 1018 hPa and minimum pressure of 1009 hPa.

At buoy 46027, the pressure minimum occurred at 0100 UTC 16 May and was followed by two pressure rises for both the simulation and observation, although the simulated pressure variation was smoother than the observed one. At Cape Arago, both the simulated and observed pressure was about 1024 hPa at 0600 UTC 15 May. Both pressures fell rapidly during the next 20-h and then remained relatively constant for about 18 h. Subsequent to this, both pressures rose and reached their maxima with a rate 0.40 hPa h^{-1}. Again, the simulated pressure variation matched reasonably well with the observation except that the simulated pressure maximum was smaller than the observed one. The modeled pressure at Cape Arago showed that there was a pressure trough followed by a jump in pressure. This feature, which was associated with the CTD, moved northward and passed through the remaining stations for both the simulation and observations. The amplitude of the trough and subsequent pressure rise appeared to diminish along the northern coast at, and north of, Destruction Island (Figs. 14 and 15). Further comparison of Figs. 14 and 15 suggests that the model pressure rise at many of the stations between Cape Arago and Estevan Point (e.g., Hoquiam) is not quite as sharp as that observed.

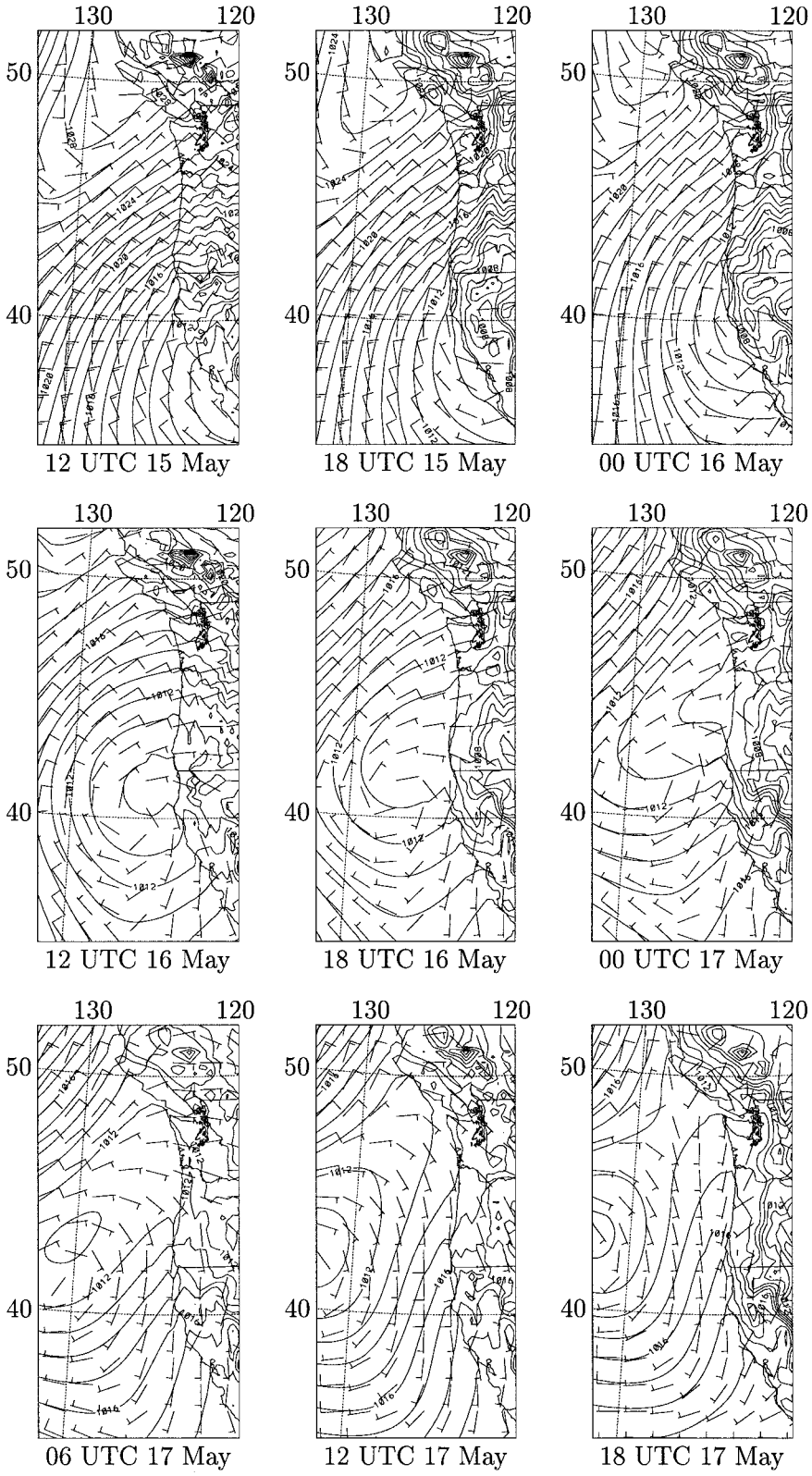

FIG. 8. Simulated sea level pressure and wind field at 109.7 m above the surface for the event of 15–17 May 1985 from grid 2 with horizontal resolution of 25 km. For clarity, every fifth wind vector in both dimensions is plotted. Contour interval is 1 hPa.

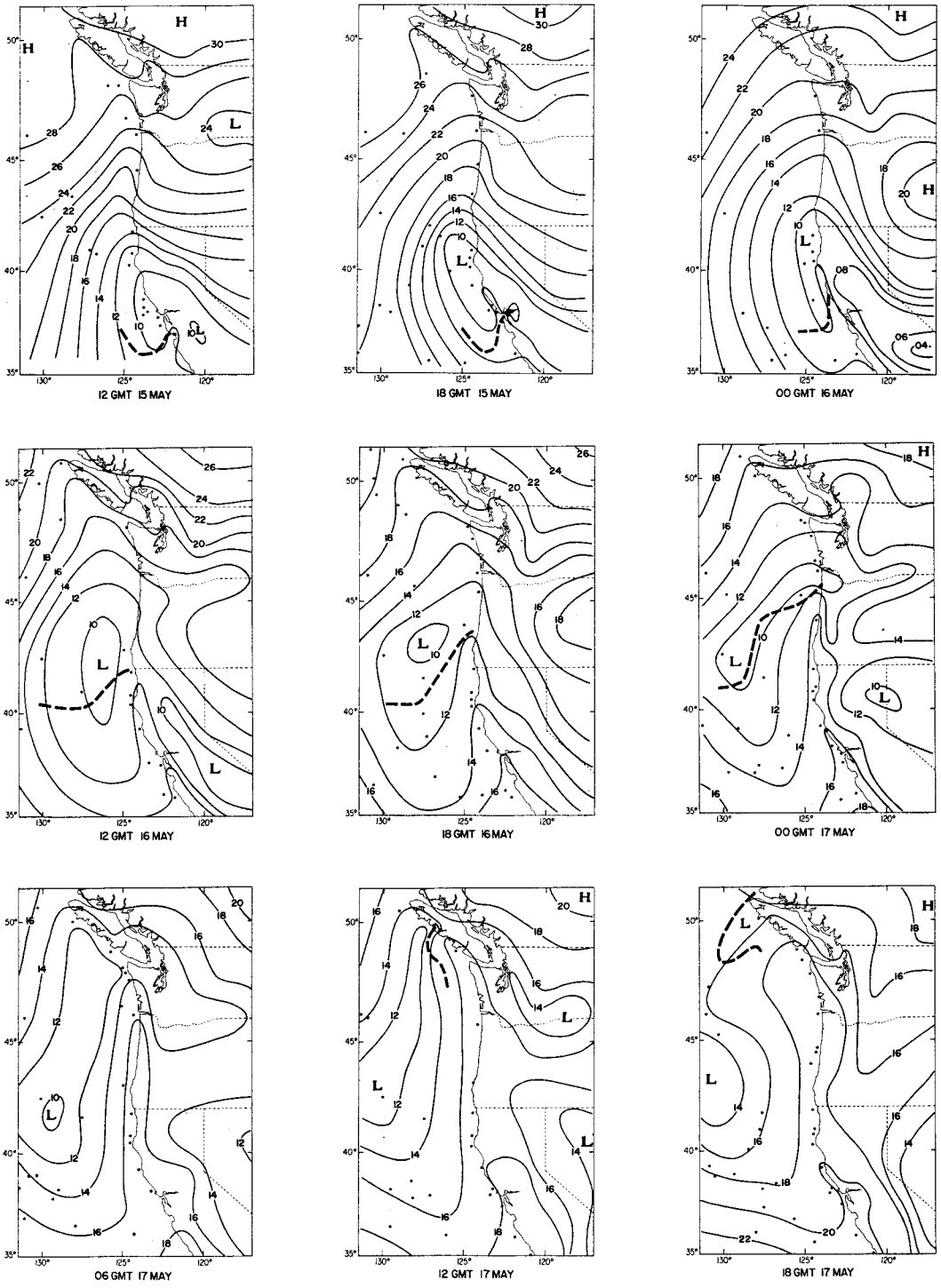

FIG. 9. Mesoscale sea level pressure analyses for the same times as in Fig. 8 (reproduced from Fig. 9 in MA87). Heavy dashed lines are the northern boundaries of the coastal stratus, based on GOES imagery. Isobars are 10*xx* hPa. Observations over the Pacific Ocean are indicated by solid dots.

We attribute this deficiency of the model to its difficulty in capturing details of the boundary layer dynamics, which in turn arises from the lack of sufficiently high-resolution boundary layer data in the standard level NCEP initialization fields. Were such high-resolution initialization data available, it is possible that the model simulations here may have been able to capture more of the steep leading edge of the gravity current–like

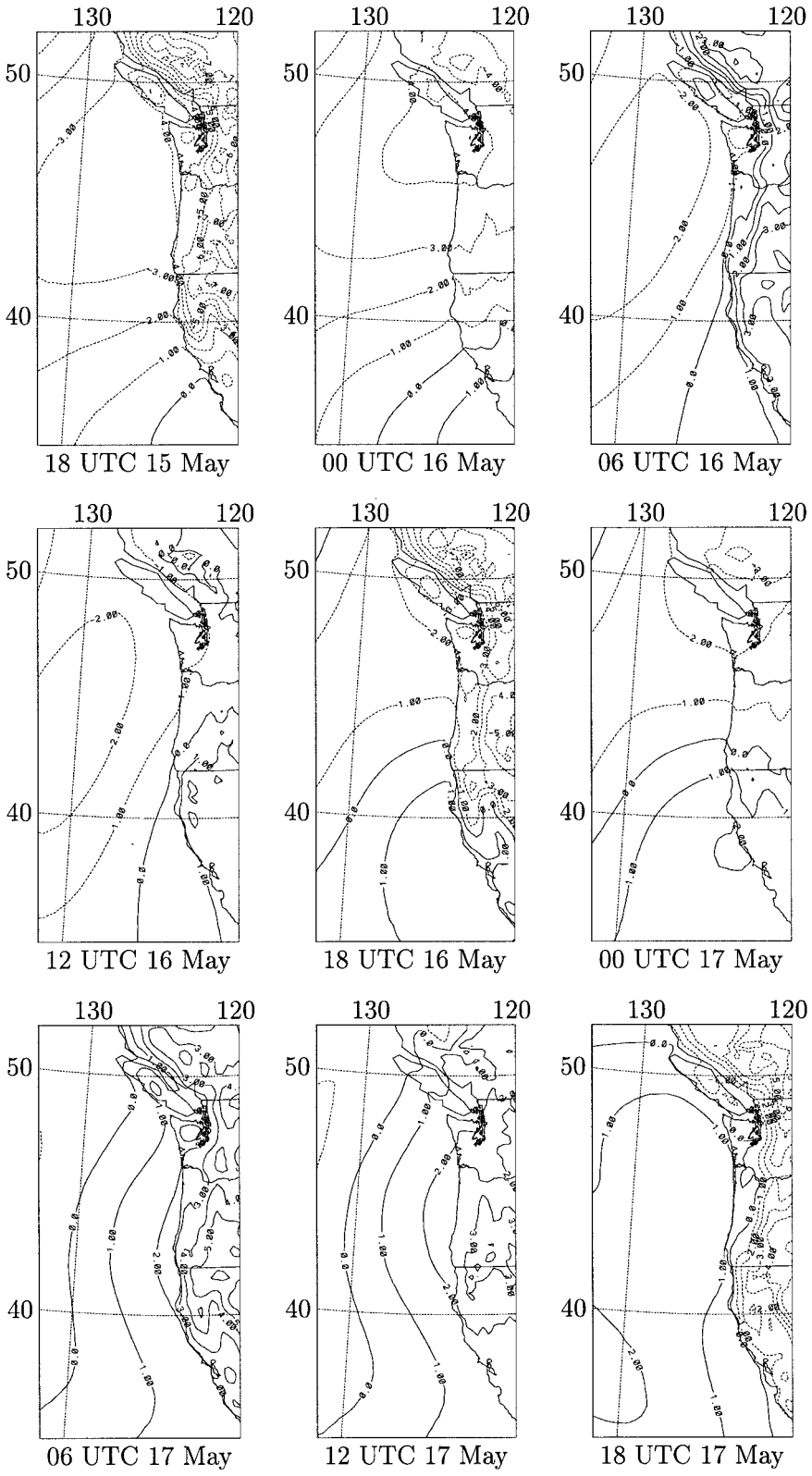

FIG. 10. Six-hour pressure changes of the simulated sea level pressures for the event of 15–17 May 1985 from grid 2 of RAMS. Contour interval is 1 hPa (6 h)$^{-1}$. Falling pressure is indicated by dashed lines.

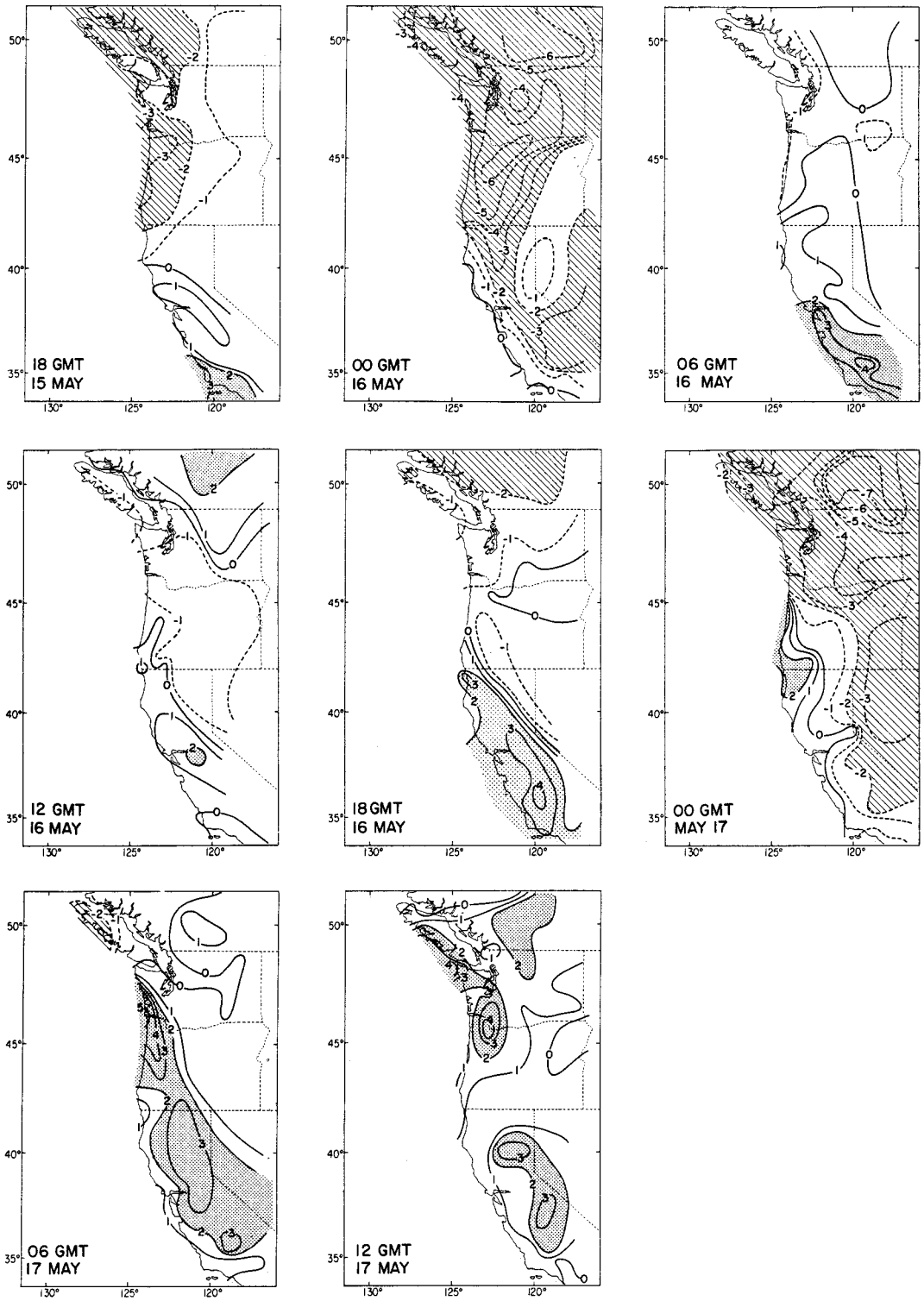

FIG. 11. Observed 6-h pressure changes for the same times as in Fig. 10 (reproduced from Fig. 11 in MA87).

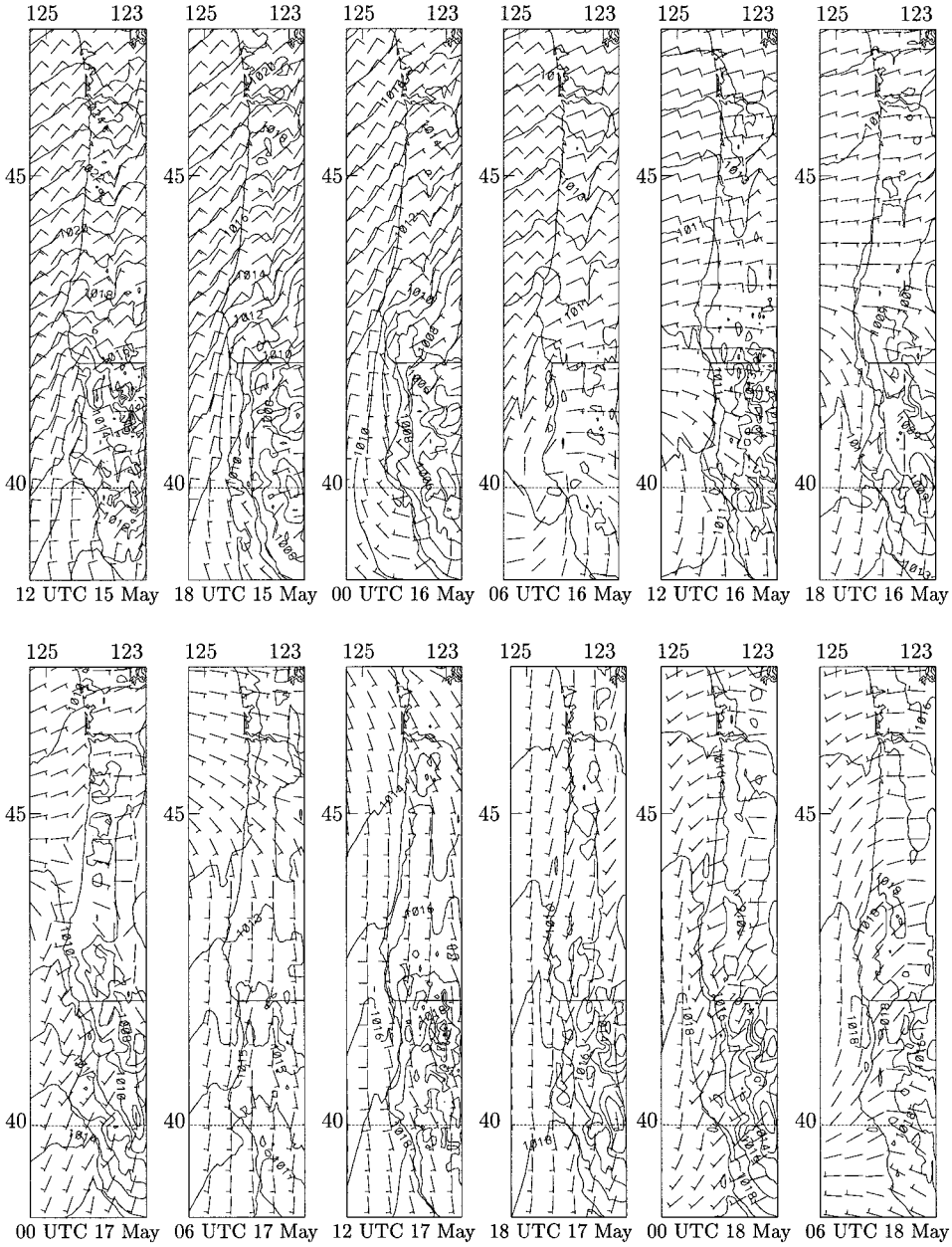

FIG. 12. Simulated sea level pressure and winds at 108.4 m ASL from 1200 UTC 15 May through 0000 UTC 18 May 1985 from grid 3 with a horizontal grid spacing of 6.25 km. For clarity, every ninth wind vector in both dimensions is plotted. Contour interval is 1 hPa.

CTD than is shown in Fig. 14. For example, various idealized simulations with the model forced by a cooling in the lowest 1.3 km of the coastal atmosphere in the southern part of the domain indicated that the model was able to simulate the steep leading edge of the resulting gravity current–like CTD. Although there are some differences between model and observations in the minimum and maximum pressures, and the rate of pressure increase, Figs. 14 and 15 suggest that the simulated CTD and its propagation through the various stations agreed reasonably well with observations.

Time series of modeled and observed pressure gradients, sea level pressure, temperature, and wind components at buoy 46027 and Hoquiam are shown in Figs. 16 and 17. At buoy 46027, the pressure, its alongshore gradient, and the u, v wind components are in reasonable agreement with observation, while the observed temperature is cooler than modeled, at times by as much as 6°C. At Hoquiam (Fig. 17) the observed pressure is consistently higher than modeled by about 4 hPa. The modeled pressure difference is consistently negative, indicating higher pressure to the south, whereas the ob-

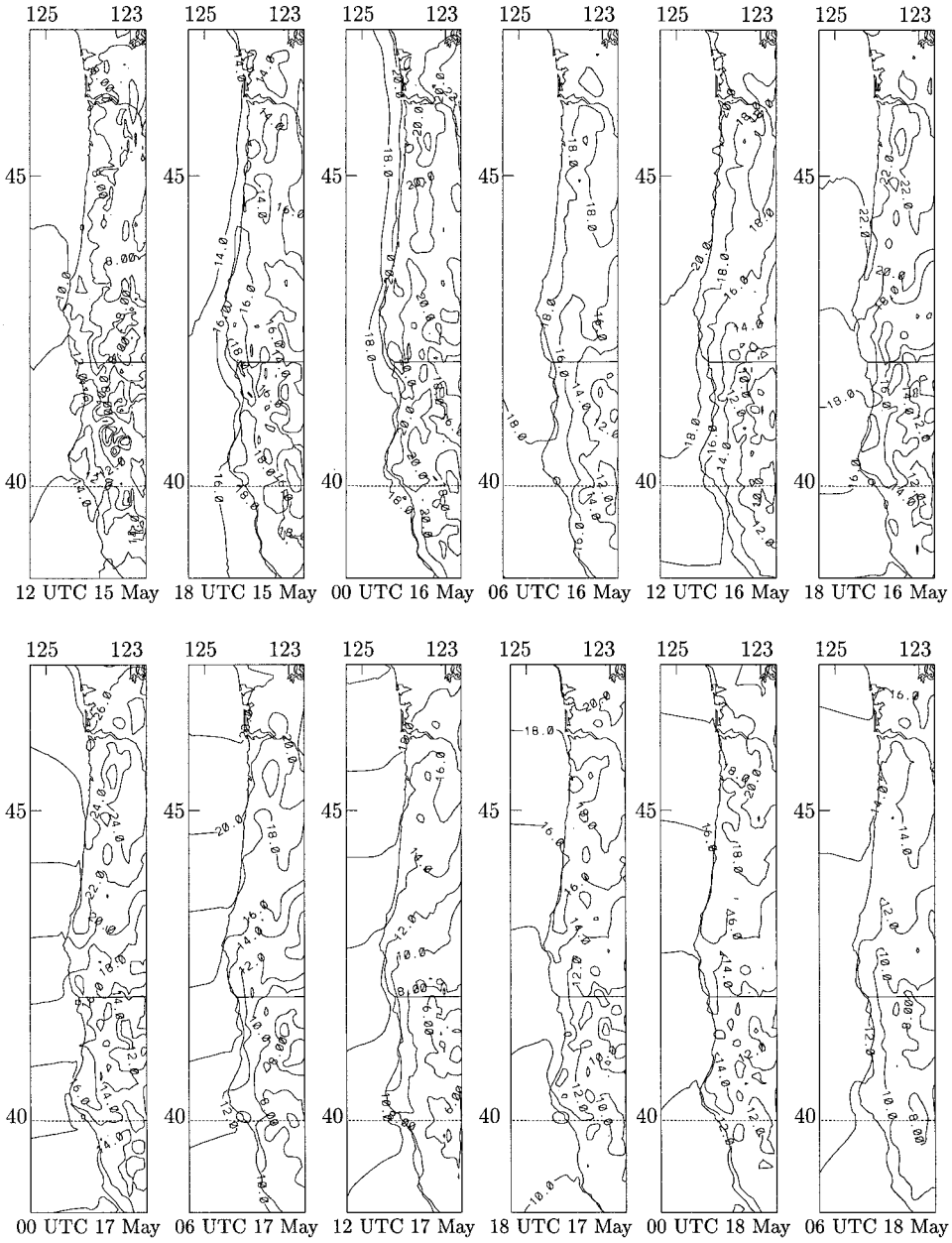

FIG. 13. Simulated near-surface temperatures at 108.4 m ASL from 1200 UTC 15 May through 0000 UTC 18 May 1985 from grid 3 with horizontal grid spacing of 6.25 km. Contour interval is 2°C.

served pressure difference is near zero or positive, indicating higher pressure to the north. The modeled and observed temperatures are in closer agreement and the wind components are reasonably similar. We attribute the difference between modeled and observed temperature over water (at buoy 46027) to the relatively poor simulation of the boundary layer (which we have suggested results from insufficient vertical resolution in the NCEP initialization fields). The difference between modeled and observed pressure and pressure gradients at Hoquiam is a previously noted consequence of the leading edge of the simulated coastal ridge being somewhat less steep than observed, which again results from the deficiencies in the modeled boundary layer.

Figure 18 presents the latitude where the transition from northerlies to southerlies occurred as a function of time for both the simulation and observations. The simulated southerly transition during the CTD event traveled northward from southern California. It moved quickly along the coast of southern and central California but slowed down between about San Francisco and Cape Mendocino during 0000–0900 UTC 16 May.

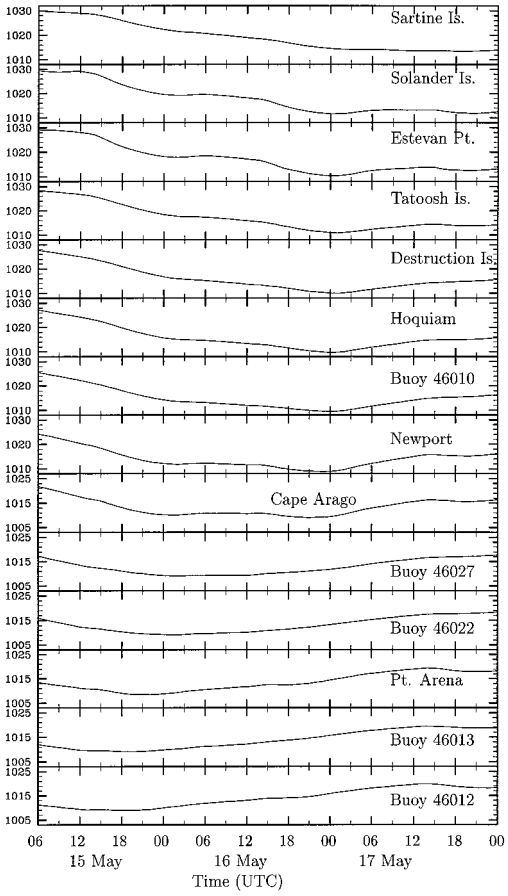

FIG. 14. Simulated time evolution of sea level pressure at a series of coastal stations and buoys from central California to the northern tip of Vancouver Island from grid 2.

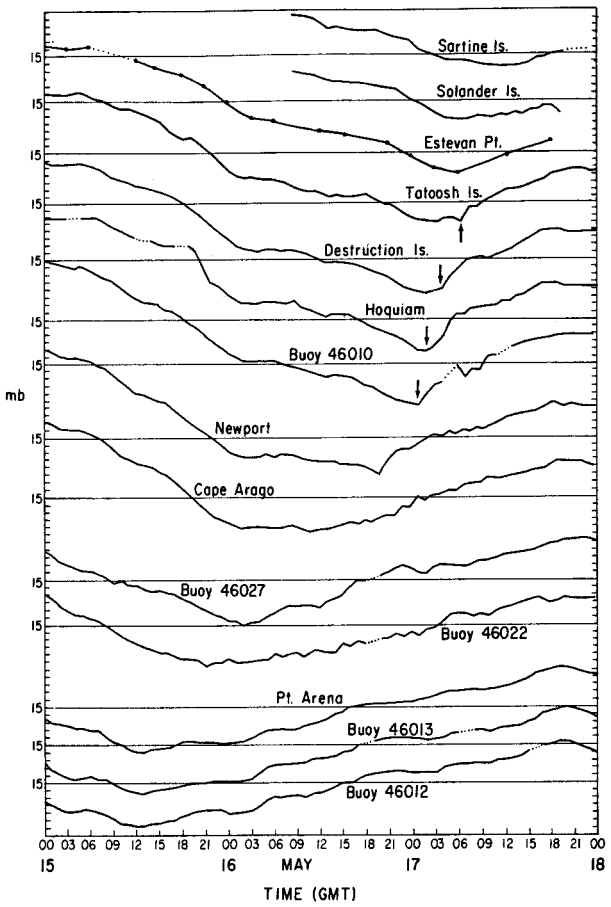

FIG. 15. Observed evolution of sea level pressure at a series of coastal stations as in Fig. 14 (Reproduced from Fig. 12 in MA87).

The wind shift then propagated quickly again during 1000–1200 UTC May 16 near buoy 46022 on the northern California coast, before slowing during 2000–2400 UTC 16 May along the coast of central Oregon. For the remainder of the event, the southerly transition moved rapidly northward along the Washington and Vancouver Island coasts. Comparison of the simulated transition with observations (Fig. 18) suggests qualitative agreement between modeled and observed wind transitions. In particular, modeled and observed locations of observed rapid transition (indicated by a more vertical line in Fig. 18) correspond quite well. The simulated transition lagged the observed transition, by a few hours, and in some places by as much as 10 h. The largest time lags occur when the observed transition is nearly instantaneous, and the modeled transition, while showing an increase in speed, is slower. It seems that the variations in propagation speed of the southerly transition are due either to temporal changes in synoptic forcing or to an interaction between the propagating disturbance and complex coastal terrain.

e. Vertical profiles

Observed and simulated vertical profiles for Vandenberg and Quillayute are shown in Figs. 19 and 20. The simulated vertical profile for Quillayute is from the northern part of grid 3, while the simulated profile for Vandenberg is from grid 2 since the grid 3 domain does not extend far enough south. While the mean temperature of the simulated profiles are mostly consistent with observations, the modeled profiles are smoother and have a less distinct marine boundary layer than observations suggest. This is particularly true at Quillayute (Fig. 20) after 1200 UTC 17 May when the observed deep inversion layer is not simulated. The simulated vertical wind profiles are quite close in magnitude, direction, and depth to the observed profiles at both Vandenberg and Quillayute. The simulated moisture profiles did not capture the thin saturated layer present in several of the observed profiles. We attribute this to the lack of sufficiently high-resolution moisture information in the NCEP fields used for model initialization. The model seems poorest at simulating the planetary boundary layer (PBL) when the low-level flow is onshore and is being cooled from below by the sea surface. The model PBL

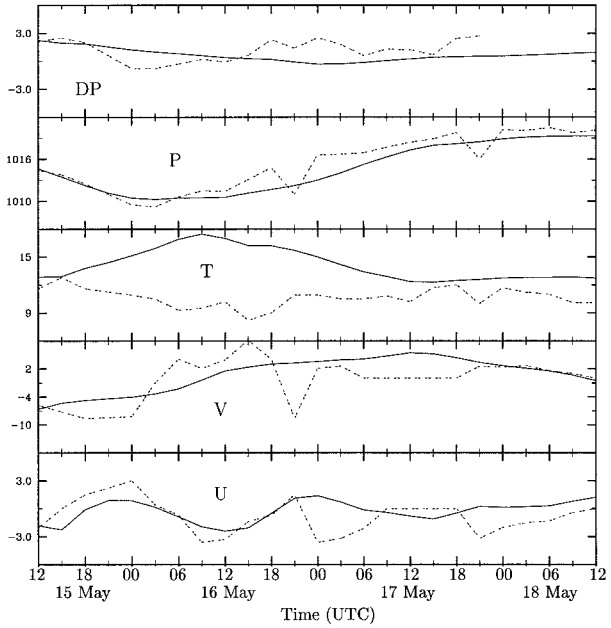

FIG. 16. For buoy 46027 the observed (dashed line) and simulated (solid line): DP is the sea level pressure at buoy 46027 minus that at buoy 46022 (hPa), *P* is the sea level pressure (hPa), *T* is the surface temperature (°C), *V* is the northward wind component (m s^{-1}), and *U* is the eastward wind component (m s^{-1}).

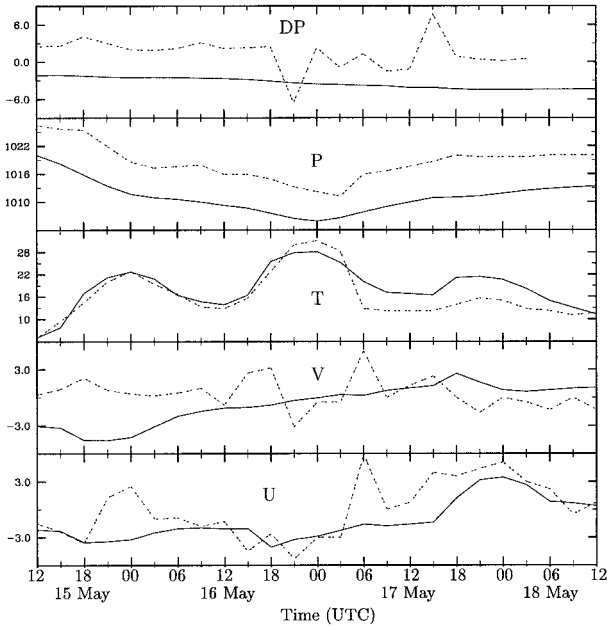

FIG. 17. For Hoquiam the observed (dashed line) and simulated (solid line): *DP* is the sea level pressure at Hoquiam minus that at buoy 46010 (hPa), *P* is the sea level pressure (hPa), *T* is the surface temperature (°C), *V* is the northward wind component (m s^{-1}), and *U* is the eastward wind component (m s^{-1}).

problem does not seem to be related to vertical resolution of this PBL. For example at Quillayute (Fig. 20), the vertical profile from grid 3, which has a vertical resolution of 18.75 m near the surface, was found to improve only slightly on the vertical profile from grid 2, which has a vertical resolution of 75 m near the surface.

4. Discussion

The CTD of 15–17 May 1985 brought an abrupt change in wind direction and speed, a precipitous temperature drop, and a sharp rise in sea level pressure along the western coast of North America. MA87 have analyzed this vigorous CTD based on all available observed data. In this paper, a simulation of this particular event with the RAMS mesoscale numerical model has been compared with the observations in MA87. Two-way interactive grid nesting in the model allows local fine-mesh grids to resolve the mesoscale structure of CTD while simultaneously modeling the synoptic-scale environment of the system on a coarser grid. With typical across-shore length scales on the order of 100 km, a horizontal grid spacing of 25 km (grid 2) is just able to resolve a CTD, while the grid 3 horizontal spacing of 6.25 km provides much improved resolution of the CTD. With marine boundary layer depths of a few hundred meters, the vertical resolution of this simulation (near the surface—75 m for grids 1 and 2 and 18.75 m for grid 3), particularly in grid 3, should be able to adequately resolve trapped disturbances in the boundary layer.

As expected, the simulation on grid 1 (horizontal resolution 100 km) matches the NCEP synoptic data very well. Grids 2 and 3, with horizontal resolution of 25 and 6.25 km, respectively, show a reasonable cor-

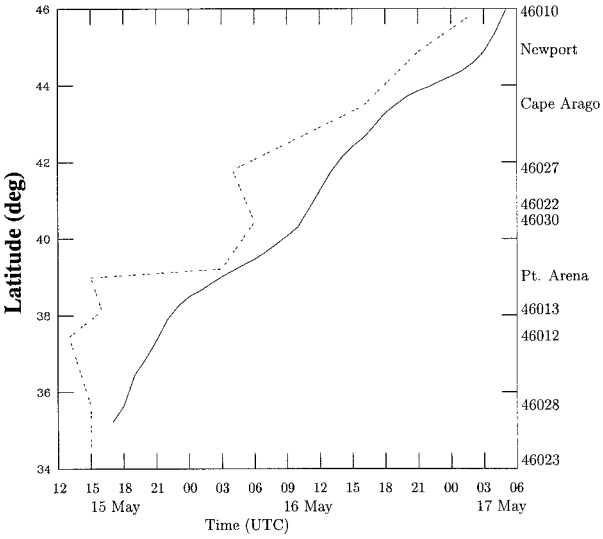

FIG. 18. The observed (dashed line) and grid 2 simulated (solid line) position of the southerly transitions as a function of time.

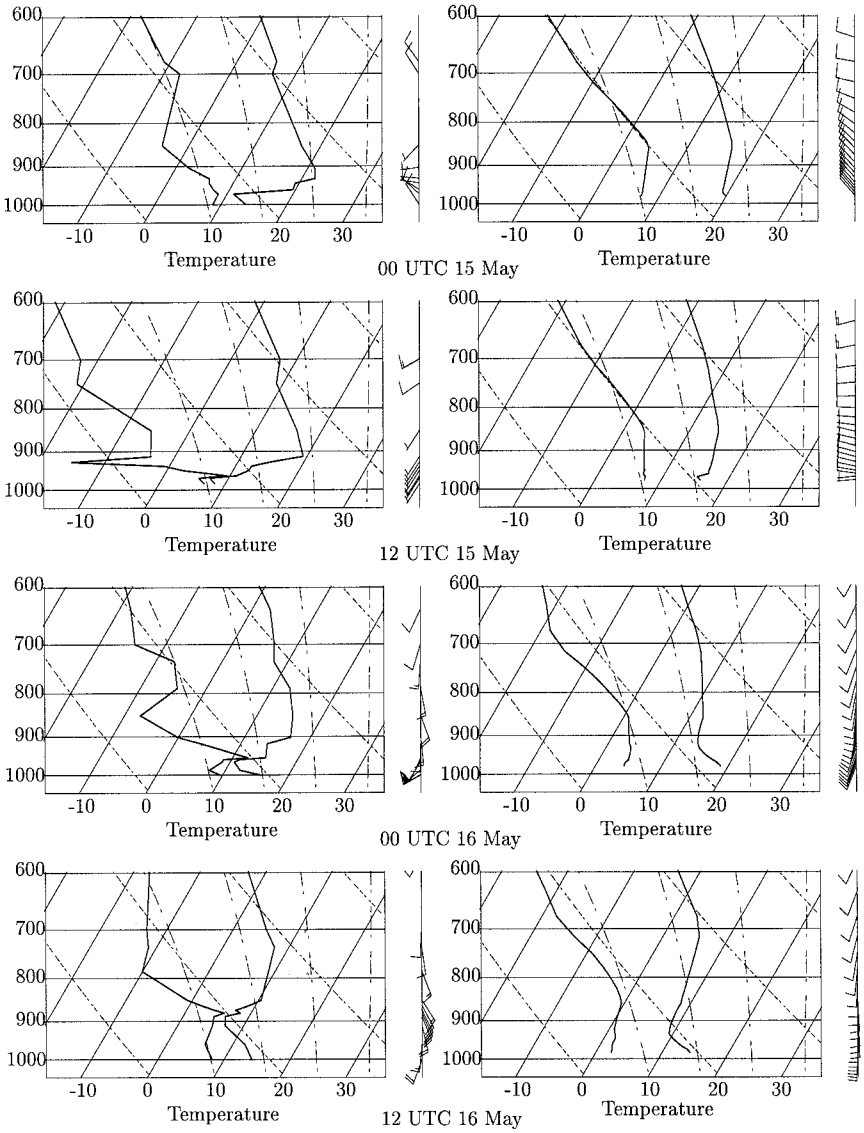

FIG. 19. Simulated (right) and observed (left) vertical profiles of temperature, dewpoint, and wind for Vandenberg.

respondence with the mesoscale observational analysis reported in MA87. A significant difficulty in attempting to simulate the mesoscale characteristics is that the observations are not of sufficiently high temporal and spatial resolution to enable the model initialization and subsequent simulation to reach its optimum. This is particularly problematic in initializing the model with an adequate marine boundary layer structure. Since the marine boundary layer is not present in the NCEP initialization data, it is not well represented in the RAMS simulation either, despite the fact that the enhanced vertical resolution should be sufficient to simulate it. Very recent simulations, to be discussed in a companion paper, indicate that the weak nudging toward NCEP conditions in the interior of the model domain also degraded the simulated marine boundary layer. In spite of the poor marine boundary layer representation, the model was able to simulate the coastal ridge development and progressive transition to southerly flow. This model's result therefore suggests that the mesoscale response of the lower atmosphere to the synoptic forcing and the evolution of that forcing was more important than boundary layer dynamics for the CTD evolution during the May 1985 case. The synoptic forcing that seems most important in the formation and northward propagation of this CTD was the westward migration of a cold low at the surface and upper levels across the northern California–southern Oregon coast. This resulted in onshore flow and ridging at the surface in the south, and offshore flow and warming to the

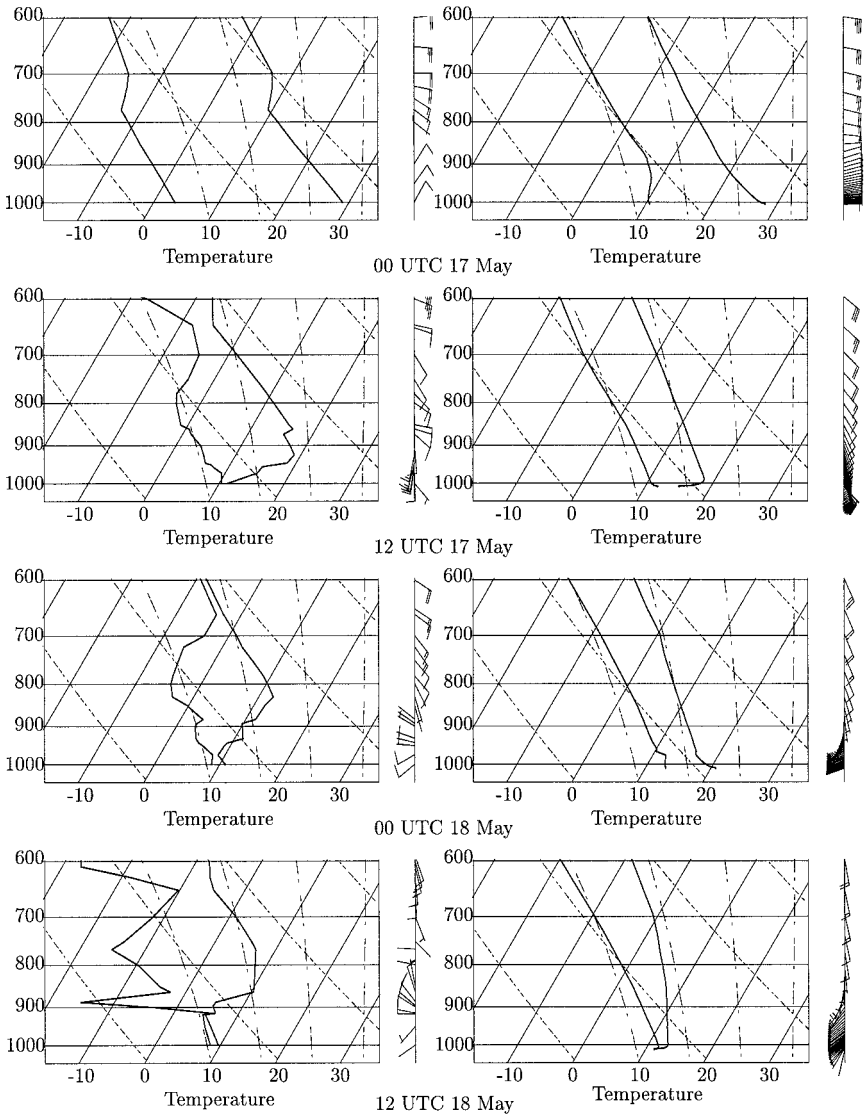

FIG. 20. Simulated (right) and observed (left) vertical profiles of temperature, dewpoint, and wind for Quillayute.

north. It should be stressed that the May 1985 case was a strong event, both in terms of the synoptic forcing and the resulting weather changes in the lower atmosphere and that the importance of synoptic versus boundary layer effects may very well be different for other CTD events.

The current study has demonstrated that the RAMS model can be successfully applied to simulating an observed CTD event. A companion study is aimed at analyzing the mesoscale dynamics of this event in more detail by means of a force balance analysis of the RAMS model fields. The ability of the RAMS model to simulate an observed case study, as performed here, represents an important step forward in our ability to understand and, eventually, accurately forecast these events. Furthermore, it lays the groundwork for future studies aimed at investigating the sensitivity of these events to variability in the topography, surface fluxes, and background synoptic conditions, all factors suggested by previous observational studies as being important in CTD evolution and decay.

Acknowledgments. Support for this project came from the U.S. Office of Naval Research Coastal Meteorology Accelerated Research Initiative Grant 96pr01929-00. RAMS was developed under the support of the National Science Foundation (NSF) and the U.S. Army Research Office (ARO). We would like to acknowledge the helpful suggestions made by three anonymous reviewers of this paper.

REFERENCES

Abbs, D. J., and R. A. Pielke, 1987: Numerical simulations of orographic effects on NE Colorado snowstorms. *Meteor. Atmos. Phys.,* **37,** 1–10.

Bond, N. A., C. F. Mass, and J. E. Overland, 1996: Coastally trapped wind reversals along the United States west coast during the warm season. Part I: Climatology and temporal evolution. *Mon. Wea. Rev.,* **124,** 430–445.

Clark, T. L., and R. D. Farley, 1984: Severe downslope windstorm calculations in two and three spatial dimensions using anelastic interactive grid nesting: A possible mechanism for gustiness. *J. Atmos. Sci.,* **41,** 329–350.

Dorman, C. E., 1985: Evidence of Kelvin waves in California's marine layer and related eddy generation. *Mon. Wea. Rev.*, **113,** 827–839.

——, 1987: Possible role of gravity currents in northern California's marine layer and related eddy generation. *J. Geophys. Res.*, **92,** 1497–1506.

——, 1988: Comments on ''Coastal southerlies and alongshore surges of the west coast of North America: Evidence of mesoscale topographically trapped response to synoptic forcing.'' *Mon. Wea. Rev.,* **116,** 2401–2406.

Gill, A. E., 1977: Coastally trapped waves in the atmosphere. *Quart. J. Roy. Meteor. Soc.,* **103,** 431–440.

Holland, G. J., and L. M. Leslie, 1986: Ducted coastal ridging over S.E. Australia. *Quart. J. Roy. Meteor. Soc.,* **112,** 731–748.

Jackson, P. L., and D. G. Steyn, 1994: Gap winds in a fjord. Part I: Observations and numerical simulation. *Mon. Wea. Rev.*, **122,** 1245–1265.

Klemp, J. B., R. Rotunno, and W. C. Skamarock, 1995: Shallow-water model simulations of coastally trapped disturbances. Preprints, *Seventh Conf. on Mountain Meteorology*, Breckenridge, CO, Amer. Meteor. Soc., 197–202.

Lee, T. J., R. A. Pielke, R. C. Kessler, and J. F. Weaver, 1989: Influence of cold pools downstream of mountain barriers on downslope winds and flushing. *Mon. Wea. Rev.,* **117,** 2041–2058.

Mass, C. F., and M. D. Albright, 1987: Coastal southerlies and alongshore surges of the west coast of North America: Evidence of mesoscale topographically trapped response to synoptic forcing. *Mon. Wea. Rev.,* **115,** 1707–1738.

——, and ——, 1988: Reply. *Mon. Wea. Rev.,* **116,** 2407–2410.

——, ——, and D. J. Brees, 1986: The onshore surge of marine air into the Pacific Northwest: A coastal region of complex terrain. *Mon. Wea. Rev.,* **114,** 2602–2627.

Pielke, R. A., and Coauthors, 1992: A comprehensive meteorological modeling system—RAMS. *Meteor. Atmos. Phys.,* **49,** 69–91.

Reason, C. J. C., 1994: Orographically trapped disturbances in the lower atmosphere: Scale analysis and simple models. *Meteor. Atmos. Phys.,* **53,** 131–136.

——, and M. R. Jury, 1990: On the generation and propagation of the southern African coastal low. *Quart. J. Roy. Meteor. Soc.,* **116,** 1133–1151.

——, and D. G. Steyn, 1990: Coastally trapped disturbances in the lower atmosphere: Dynamic commonalities and geographic diversity. *Prog. Phys. Geogr.,* **14**(2), 178–198.

——, and ——, 1992: The dynamics of coastally trapped mesoscale ridges in the lower atmosphere. *J. Atmos. Sci.,* **49,** 1677–1692.

——, and R. Dunkley, 1993: Coastally trapped stratus events in British Columbia. *Atmos.–Ocean,* **31,** 235–258.

Rogerson, A. M., and R. M. Samelson, 1995: Synoptic forcing of coastal-trapped disturbances in the marine atmospheric boundary layer. *J. Atmos. Sci.,* **52,** 2025–2040.

Xian, Z., and R. A. Pielke, 1991: The effects of width of land masses on the development of sea breezes. *J. Appl. Meteor.*, **30,** 1280–1304.